Scanning Acoustic Microscopy Comparison of Descemet's Membrane Normal Tissue and Tissue With Fuchs' Endothelial Dystrophy

Esam T. Ahmed Mohamed,[1] Jean-Marc Perone,[2] Sebastian Brand,[3] Michael Koegel,[3] and Nico F. Declercq[1]

[1]Laboratory for Ultrasonic Nondestructive Evaluation "LUNE", UMI Georgia Tech–CNRS 2958, Metz, France
[2]Ophthalmology Department of the Regional Hospital Center of Metz-Thionville, Mercy Hospital, Metz, France
[3]Fraunhofer Institute for Microstructure of Materials and Systems IMWS, Center for Applied Microstructure Diagnostics CAM, Halle, Germany

Correspondence: Esam T. Ahmed Mohamed, Laboratory for Ultrasonic Nondestructive Evaluation "LUNE", UMI Georgia Tech–CNRS 2958, 2 rue Marconi, Metz 57070, France; eahmedm@georgiatech-metz.fr.

Submitted: August 17, 2018
Accepted: October 18, 2018

Citation: Ahmed Mohamed ET, Perone J-M, Brand S, Koegel M, Declercq NF. Scanning acoustic microscopy comparison of Descemet's membrane normal tissue and tissue with Fuchs' endothelial dystrophy. *Invest Ophthalmol Vis Sci*. 2018;59:5627–5632. https://doi.org/10.1167/iovs.18-25516

Purpose. To describe the application of scanning acoustic microscopy in the GHz-range (GHz-SAM) for qualitative imaging and quantitative characterization of the micromechanical properties of the Descemet's membrane and endothelial cells of cornea tissue.

Methods. Investigated were samples of a normal tissue and a tissue with Fuchs' endothelial dystrophy (FECD, cornea Guttata). Descemet's membranes were fixed on glass substrates and imaged utilizing a focused acoustic lens operating at a center frequency of 1 GHz.

Results. GHz-SAM data, based on the well-established $V(z)$ technique, revealed discrepancies in the velocity of the propagation of Rayleigh surface acoustic waves (RSAW). RSAW were found to be slower in glass substrates with FECD samples than in the same glass substrates (soda-lime) with normal Descemet membrane, which indicates lower shear and bulk moduli of elasticity in tissues affected by FECD.

Conclusions. Noninvasive/nondestructive GHz-SAM, is utilized in this study for the imaging and characterization of Descemet membranes, fixated on glass substrates. $V(z)$ signatures containing sufficient oscillations were obtained for the system of Descemet membranes on glass substrates. The observed variation in the microelastic properties indicates potential for further investigations with GHz-SAM based on the V(z) technique.

Keywords: GHz-SAM, quantitative biomechanics, FECD, Descemet membrane, endothelial cells

Fuchs' endothelial dystrophy (FECD) is a corneal disease accompanied by abnormality of the Descemet membrane indicated by polymegethism (irregularly shaped cells) and polymorphism (variable shape of cells) in addition to a considerable loss of the multifunctional, nondegenerative, corneal endothelial cells.[1–3] The progressive decrease of cell density is accompanied by an increase in the deposition of the extracellular matrix and thickening of Descemet membrane that accumulates in the form of granular guttae leading to corneal edema and decreased visual acuity.[3,4] FECD is associated with genetic mutations,[4–7] as well as environmental influences,[7] age and sex[8] among other possible factors.

In recent years, many techniques have been employed for encoding the pathology and physiology of FECD. Besides molecular genetic techniques,[5] confocal and specular microscopy,[1,9] retroillumination photography,[10] and optical coherence tomography were used to follow pathomorphologic changes in FECD.[11] Different approaches were also involved to elucidate the biomechanical basis of FECD. Ultrasonic pachymetry, for instance, has related the thickening of the center of corneas to the degree of severity.[8] Transmission electron microscopy (TEM) and quantitative dynamic atomic force microscopy (QD-AFM) have shown that the mechanical properties as well as the internal structures of the cornea are altered considerably in FECD.[12] The biomechanics of FECD has also been studied by the ocular response analyzer (ORA). Despite these valuable efforts, the detailed mechanisms of the biomechanical alterations remain undiscovered.[12] In the presented work, SAM in the GHz-frequency band is employed for the quantitative investigation of cornea tissue (Descemet membrane) with FECD in comparison to normal cornea (Descemet membrane).

Methods

Scanning Acoustic Microscopy

Scanning acoustic microscopy in the GHz-band (GHz-SAM) enables the noninvasive and nondestructive assessment of the microelastic properties of objects including optically opaque materials and imaging with microscopic resolution in 1 μm regime without the need for histological staining. GHz-SAM is also a unique technique with respect to its superior sensitivity to surface and subsurface regions and its contrast mechanism which provides access to the mechanical properties. The comprehensive description of the working principle of the acoustic microscope can be found elsewhere.[13,14] Briefly, in a reflection acoustic microscope, a piezoelectric transducer

mounted on the back surface of an acoustic lens (mostly made of sapphire) receives a short electric RF pulse (approximately 10–30 ns in duration) that it converts into a mechanical wave. This acoustic wave then propagates through the sapphire rod and is focused sharply by the spherical cavity of the lens, located opposite to the piezo element, into a diffraction limited point. The signal that is reflected by the sample is then collected back by the acoustic lens and converted into an electric signal by the piezo element. The micrograph is then formed by scanning in two dimensions and processing the reflected signal into a grayscale map. By translating the lens perpendicular to the scan direction, an elastomechanical information about the underlying surface of the examined sample is obtained. A specific capability of SAM that enables the assessment of acoustic surface and/or interface waves is based on the variation of the reflected signal with the defocus distance of the transducer, abbreviated as $V(z)$, and called material signature, which is discussed in the following section. The contrast in SAM is generated upon the variations of several parameters of the scanned area, namely the mass density, the velocity of propagation of ultrasound which is directly related to the elastic moduli, the thickness and the topography of the examined object. The contrast is sensitive to the distance between the lens and the sample as manifested by the $V(z)$ curve which involves interference phenomena with additionally excited wave modes.[13,15,16] In a large number of scientific publications, SAM has been shown to facilitate quantitative (parametric) imaging of many biological tissues and single cells.[17–23] Recently, it has also been utilized for the mapping of the microelastic properties of cornea tissues.[24]

Output Signal Voltage in Dependence on the Defocus Distance *V*(z)

A specific feature of SAM, when strongly focused transducers are utilized for imaging, is that the imaging contrast varies considerably with the distance between the acoustic lens and the specimen, enabling the visualization of subsurface regions depending on the acoustic properties of the specimen[25] and the numerical aperture of the acoustic lens. Acoustic waves incident at the Rayleigh critical angle, excite Rayleigh surface acoustic waves (RSAW), provided that the surface of the imaged sample supports the propagation of such waves. Rayleigh waves can be excited and detected by appropriate defocusing utilizing an acoustic lens with a sufficiently large aperture opening angle that exceeds the critical angle for exciting Rayleigh waves. Figure 1 illustrates the excitation and detection of RSAW by defocusing the acoustic lens toward the sample.[26] Ray 1, which is incident on the sample at the Rayleigh angle excites a RSAW which propagates in the surface of the sample and leaks energy back into the couplant and thus, excites a compressional wave in the fluid under the Rayleigh angle. A ray that propagates along a path symmetrical to ray 1, (ray 4) to the transducer interferes with the specular ray (ray 3). The voltage value of the resulting (summed) signal, therefore depends on the lens-sample distance (z) and the wavelengths in the couplant. As the spacing "z" changes, the relative phases of the rays 1 and 4 vary, so that the superposition alternates between constructive and destructive interference. This effect considerably contributes to the contrast in the acoustic micrographs. A plot over the defocus results in an interference pattern referred to as the $V(z)$ curve containing minima and maxima according to the interference of the two wave modes.[27,28] The period of the resulting oscillations Δz, in the $V(z)$ curve, can be calculated from the phase relations and forms the base for calculating the velocity of the RSAW[26] in the sample

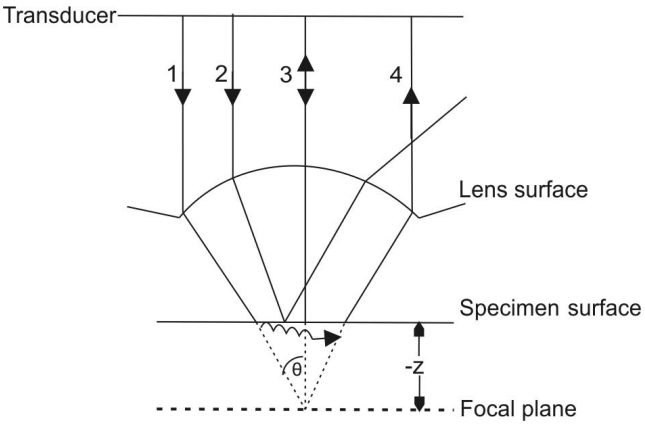

Figure 1. Illustration of the different rays that can contribute to the formation of the $V(z)$ collected by a negatively defocused lens (defocusing toward the sample).

surface. The V(z) signature can finally be presented mathematically as[29]:

$$V(z) = 2\pi \int_0^{\frac{\pi}{2}} P(\theta)R(\theta)exp[-i2kz\cos\theta]\cos\theta\sin\theta d\theta \quad (1)$$

where $P(\theta)$ is the pupil function that expresses the angular emission and detection properties of the acoustic lens, and θ as the angle of incidence. The integral in Equation 1 considers the overall geometrical contribution that ranges from 0° to the opening of the semiaperture θ_{SA}, $R(\theta)$ is the reflectance function, describing the amplitude and the phase of reflected waves as a function of the incidence angle θ, and (k) is the propagation factor, defined as $k = 2\pi f/v$, with f being the acoustic frequency and V_0 the velocity of propagation of the acoustic wave in the coupling fluid. The periodicity Δz of the oscillations in the $V(z)$ curve is defined as:

$$\Delta z = \frac{\lambda_0}{2(1 - cos\theta_R)} \quad (2)$$

where, λ_0 is the wavelength of the acoustic waves during propagation in the coupling fluid and θ_R is the Rayleigh critical angle. The velocity of propagation of the Rayleigh surface acoustic waves V_R can be expressed in terms of the ratio to the critical angle θ_R as:

$$V_R = {}^{V_0}/_{\sin\theta_R} \quad (3)$$

The velocity of Rayleigh surface acoustic waves is related to the velocity of the shear (V_s) and compressional waves (V_l) propagating in isotropic samples, for the same Possion's ratio as[29,30]:

$$\left(\frac{V_R}{V_s}\right)^6 - 8\left(\frac{V_R}{V_s}\right)^4 + 8\left[3 - 2\left(\frac{V_s}{V_l}\right)^2\right]\left(\frac{V_R}{V_s}\right)^2 - 16\left[1 - \left(\frac{V_s}{V_l}\right)^2\right] = 0 \quad (4)$$

Ultrasonic Measurements

Imaging was performed with a scanning acoustic microscope (ELSAM, Ernst-Leitz Scanning Acoustic Microscope; PVA TePla Analytical Systems, GMBH, Deutschordenstrasse 38, 73463 Westhausen, Germany), which allows imaging at a frequency

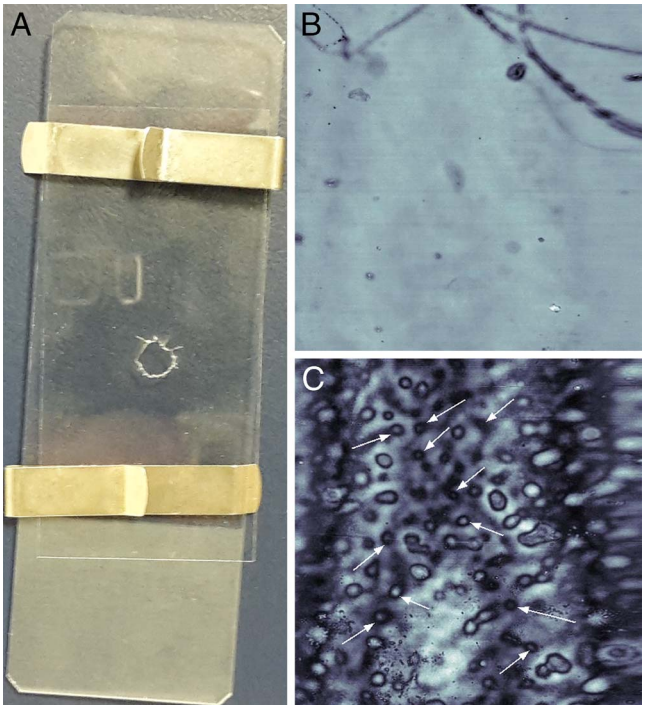

FIGURE 2. (**A**) Cornea tissue sample stabilized between a soda-lime substrate and a cover glass with 5-mm window for imaging and fixated. (**B**, **C**) Acoustic GHz-micrograph of 500 μm^2 size, recorded at 1 GHz with the acoustic lens focused on the top surface of the glass substrate for samples of normal cornea tissue (**B**) and cornea tissue with guttata (**C**). The *white arrows* in (**C**) indicate examples of guttata with the granular structures characteristic of guttata endothelia.

range of 400 MHz to 2 GHz. A stack of images was taken by scanning in C-mode, while translating the acoustic lens in axial direction which is perpendicular to the scanning plane (regarded as z-direction), starting slightly further from the focal plane and moving stepwise, passing through the focal region toward the sample ($-z$ in Fig. 1). More steps of scanning were performed in the $-z$ direction (subsurface imaging), where the corresponding $V(z)$ curves carry the information about the surface acoustic waves (SAW) and their interferences. All measurements were performed at a center frequency of 1 GHz. The stack of images in each measurement lasts about 10 minutes.

Sample Preparation

Normal Descemet membrane and endothelial cells of normal cornea tissue as well as Descemet membrane and endothelial cells affected by FECD were prepared for the acoustic GHz-microscopy inspections. A FECD sample was collected from corneal transplant surgery of a 70-year-old patient (during Descemet membrane Endothelial Keratoplasty [DMEK] procedures)[31,32] and preserved in BSS Compose solution (intraocular irrigation solution for ophthalmic surgery, isotonic saline solution; Alcon Laboratories, Rueil-Malmaison, France), whereas, the normal cornea tissue was obtained from donations (age of the donor was 75 years). The dissection of the Descemet membranes were performed manually by an experienced surgeon (J-MP) in aseptic surgical conditions and in an appropriate surgical room. Descemet membrane and endothelial corneal cells samples (corresponding to 15-µm thickness) were immobilized between soda-lime glass substrates and cover glasses with a 5 mm window which allowed scanning (maximum possible scan area was 4 mm^2) as illustrated in Figure 2A. Cornea samples were then fixated in 2% glutaraldehyde for 10 minutes. During the acoustic investigations the samples remained preserved in isotonic saline solution. The followed procedure was approved by the Regional Hospital Center of Metz-Thionville Ethic committee and by the French Ophthalmology Society Ethic Committee (IRB 00008855 Société Française d'Ophtalmologie IRB#1).

TABLE 1. The Calculated Mean Velocities of Perturbed RSAW in Glass With the Normal Descemet Membrane for Areas 1, 2, and 3 Depicted in Figure 3A

Area	Mean Value of V_R of the Glass Substrate, m/s
Region 1, the entire scan area (square 1)	2223 ± 7
Region 2 (rectangular area 2)	2223 ± 7
Region 3 (rectangular area 3)	2216 ± 7

Results and Discussion

The acoustic micrographs (Figs. 2B, 2C) are rich in contrast which implies sufficient dynamics in the acoustic and consequently in the mechanical properties of the inspected specimen. The contrast in the images is built up from a collective contribution of the variations in elasticity, density, acoustic attenuation and wave mode conversion. Figure 2B depicts a normal corneal tissue with a few number of endothelia. The morphologic changes that manifested as granular guttae are clearly evident in Figure 2C as typically reported for FECD in confocal and specular imaging.[9,33] The $V(z)$ curves shown in Figures 3B (a, b, and c), and 4B (a, b, c, and d) are the result of the interference effects between bulk waves reflected at the various interfaces and the leaky surface acoustic waves. Perturbed Rayleigh waves are excited on the glass substrate and propagate along the surface of the cornea tissue. The $V(z)$ data were extracted at different positions along the sample surface, where the tissue is perfectly aligned and no elevations are apparent. The $V(z)$ curves were utilized to comparatively investigate the microelastic properties of the cells and the formed tissue (Descemet membrane), in healthy conditions as well as in tissues with cornea Guttata. The calculated velocity of the Rayleigh waves V_R for the glass substrate beneath the cornea tissues in the areas marked by the frames and enumerated as 1 (for the entire area), 2, and 3 in Figure 3A and as 1, 2, 3, and 4 in Figure 4A are provided in Tables 1 and 2. Table 3 summarizes the calculated mean value between the normal and FECD Descemet membranes. The relatively large velocity variations between the two cases of Descemet membranes (normal and FECD), for the same substrate (soda-lime glass) and coupling fluid (saline solution), are likely attributed to the variations in the elasticity between the two tissues conditions.[34] The value of RSAWs velocity depends primarily on the shear wave velocity,[35] therefore,

TABLE 2. The Calculated Mean Velocities of Perturbed RSAW in Glass With Descemet's Membrane with FECD for Areas 1, 2, 3, and 4 Depicted in Figure 4A

Area	Mean Value of V_R of the Glass Substrate, m/s
Region 1 (rectangular area 1)	2146 ± 8
Region 2 (rectangular area 2)	2160 ± 8
Region 3 (rectangular area 3)	2158 ± 8
Region 4 (rectangular area 4)	2164 ± 8

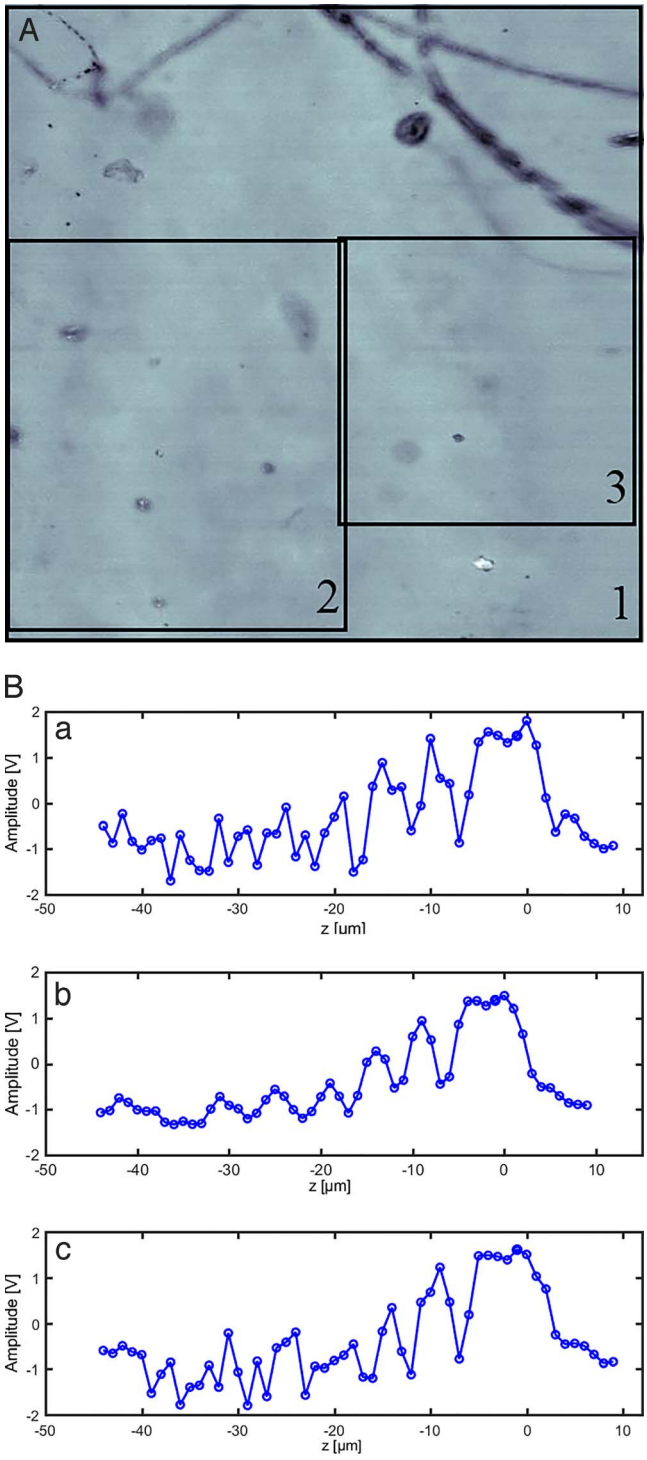

Figure 3. (**A**) The acoustic micrograph in 2A with frames indicating the regions *1*, *2*, and *3* for which $V(z)$ curves were generated. (**B**) Averaged $V(z)$ curves computed from the data taken from a stack of images for the areas marked by the frames in (**A**). Graphs **a**, **b**, **c** correspond to areas of interest *1*, *2*, *3*, respectively. The beak of amplitude at $z = 0$ μm corresponds to the collected signal when the lens was focused at the glass substrate and the oscillations at the negative defocus ($-z$) correspond to the signal collected by defocusing toward the sample.

Table 3. The Calculated Mean Velocities of Perturbed RSAW in Glass With the Normal Descemet Membrane and Descemet Membrane with FECD

Cornea Tissue	Mean Value of V_R of the Glass Substrate, m/s
Normal Descemet membrane	2221 ± 7
Descemet membrane with FECD	2168 ± 6

RSAWs are related to the shear modulus and bulk modulus of elasticity through Poisson's ratio.[29,36]

$V(z)$ is sensitive to the presence of the variations in the microstructure and the related microelasticity that are mapped in a high intensity contrast, constructing a signature of the imaged materials.[26,14] Generally, the formation of $V(z)$ curves for samples that involve soft tissues such as biological samples is influenced by the strong attenuation within these materials particularly at frequencies as high as 1 GHz.[37] Nevertheless, the observed $V(z)$ curves have sufficient oscillations. The observed $V(z)$ signature results from the interferences of the waves that are incident at a Rayleigh angle of soda-lime glass after propagating through the tissue, ensuing leaky Rayleigh waves that interfere with specular waves reflected from the different interfaces, (substrate-sample and sample-coupling fluid). The presence of the sample layer on the glass substrate causes perturbation of the Rayleigh surface acoustic wave,[38,39] so that it causes variation of the relative phase between the two signals that have the most significant contributions to the complex reflectance and consequently to the $V(z)$ (the signals from on-axis waves and waves that impinge on the glass-water interface at the Rayleigh angle) of the glass substrate. Such phase changes, are known to be sensitive to the variations in the Young's modulus and the density of the material as quantified by Maebayashi et al.[40] for thin films of polymer layers.

The variation in the biomechanical properties of the Descemet membranes of cornea tissues with guttata compared to normal membranes, has led to variations in the interference patterns and consequently in variation in the resulting $V(z)$ signature and thus, the computed velocity of propagation of the perturbed Rayleigh wave. Originally, the cornea is a viscoelastic tissue composed of collagen and cells that packed in an orderly lamellar arrangement with no blood vessels.[41] Collagen and elastin are responsible, among other constituents, for the strength and elasticity of a tissue.[42] It has been shown in previous studies that DM in normal and FECD corneas have the same collagen types but with slight discrepancy of the collagen chains.[43] DM in FECD is reported to be thicker than in normal DM. It contains abnormal posterior collagenous layers (banded and fibrillar) that account for the increase in thickness.[44] The concluded variations in the micromechanical properties could be a consequence of accumulated changes in the tissues microstructure and consequently in its microelastic properties. The biomechanical properties of cornea have been reported as being altered in cases of FECD, where a significant decrease in corneal hysteresis (CH) and corneal resistance factor (CRF) than in normal eyes with a significant elevation in the intraocular pressure (IOP_{cc}) than in normal cases have been quantified.[45] Corneal dehydration, which is normally performed by the endothelia of the normal corneas by functioning as both a barrier to fluid movement into the cornea and as an active pump that moves ions[46] and draws water osmotically from the stroma into the aqueous humor, is known to be altered in FECD. The reduced corneal endothelium cell density in FECD results in a decrease of the dehydration capacity[46,47] which likely contributes to a decreased stiffness (Young's modulus) of Descemet membrane

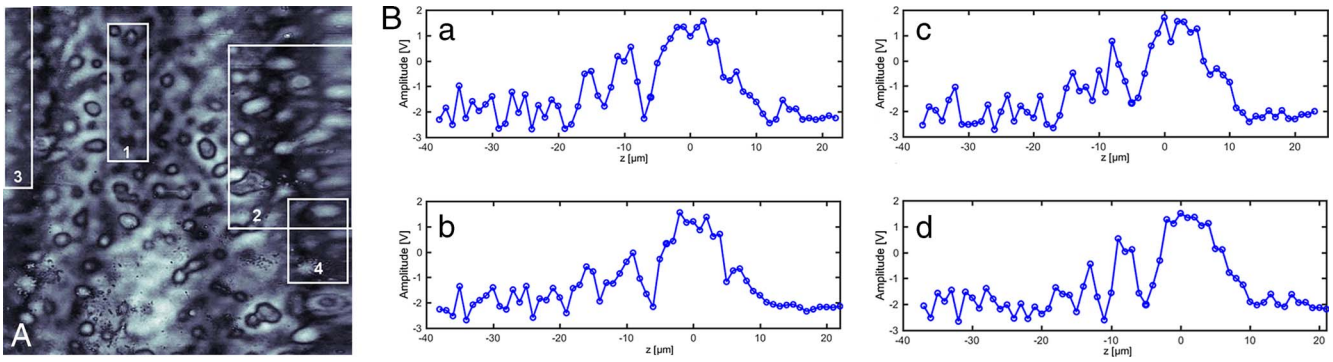

FIGURE 4. (**A**) The acoustic micrograph in 2A with frames showing the regions *1*, *2*, *3*, and *4* for which $V(z)$ curves were generated. (**B**) Averaged $V(z)$ curves computed from the data taken from a stack of images obtained for the areas marked by the frames in (**A**). Graphs **a**, **b**, **c**, **d** correspond to areas of interest *1*, *2*, *3*, *4*, respectively. The beak of amplitude at $z = 0$ μm corresponds to the collected signal when the lens was focused at the glass substrate and the oscillations at the negative defocus ($-z$) correspond to the signal collected by defocusing towards the sample.

with FECD.[48] FECD is also known to develop edema that is clinically detectable only at the most advanced grade.[46] The decreased elasticity in Descemet membrane with FECD observed in the present study, can likely be attributed to the structural changes induced by FECD in to the Descemet membrane that are known to result in a decreased stiffness in terms of Young's modulus of elasticity.[12]

CONCLUSIONS

The present work aims to contribute to gaining a further understanding of the alterations in the biomechanical properties in Descemet membranes with FECD. $V(z)$ signatures containing sufficient oscillations were obtained for the system of Descemet membranes on glass substrates. The observed discrepancies in the propagation velocity of perturbed RSAW of the glass substrate, between the two cases (glass with normal Descemet membranes and glass with Descemet membranes that has guttata), which is related to a corresponding variation in the microelastic properties, indicate potential for further investigations based on the $V(z)$ technique. The observations described here may direct further attention to the influence of the changes in the micromechanical properties of FECD in inducing, promoting, or distinguishing FECD.

Acknowledgments

The authors thank the established research partnership of Georgia Tech Lorraine and Regional Hospital Center of Metz-Thionville, Mercy Hospital in Metz.

Supported by an ARVO Publications Grant.

Disclosure: **E.T. Ahmed Mohamed**, None; **J.-M. Perone**, None; **S. Brand**, None; **M. Koegel**, None; **N.F. Declercq**, None

References

1. Bourne WM, Nelson LR, Hodge DO. Central corneal endothelial cell changes over a ten-year period. *Invest Ophthalmol Vis Sci*. 1996;38:779–782.
2. Zoega MG, Arnarsson A, Sasaki H, Söderberg GP, Jonasson F. The 7-year cumulative incidence of cornea guttata and morphological changes in the corneal endothelium in the Reykjavik Eye Study. *Acta Ophthalmol*. 2013;91:212–218.
3. Moshirfar M, Feiz V, Feilmeier MR, Kang CP. Laser in situ keratomileusis in patients with corneal guttata and family history of Fuchs' endothelial dystrophy. *J Cataract Refract Surg*. 2005;3112:2281–2286.
4. Vedana, G, Villarreal G Jr, Jun AS. Fuchs endothelial corneal dystrophy: current perspectives. *Clin Ophthalmol*. 2016;201:321–330.
5. Akimune C, Watanabe H, Maeda N, et al. Corneal guttata associated with the corneal dystrophy resulting from a βig-h3 R124H mutation. *Br J Ophthalmol*. 2000;84:67–71.
6. Hussain E, Behrooz A, Jurkunas VU. Fuchs endothelial corneal dystrophy. *Ocul Surf*. 2009;42:115–125.
7. Hamill CE, Schmedt T, Jurkunas U. Fuchs endothelial cornea dystrophy: a review of the genetics behind disease development. *Semin Ophthalmol*. 2013;28:281–286.
8. Kopplin LJ, Przepyszny K, et al. Relationship of Fuchs' endothelial corneal dystrophy severity to central corneal thickness. *Arch Ophthalmol*. 2013;130:433–439.
9. Chiou C G-YA, Kaufman SC, Beuerman RW, Ohta T, Soliman H, Kaufman HE. Confocal microscopy in cornea guttata and Fuchs' endothelial dystrophy. *Br J Ophthalmol*. 1999;83:185–189.
10. Eghrari AO, Garrett BS, Mumtaz AA, et al. Retroillumination photography analysis enhances clinical definition of severe Fuchs corneal dystrophy. *Cornea*. 2015;3412:1623–1626.
11. Kaluzny BJ, Szkulmowska A, Szkulmowski M, Bajraszewski T, Kowalczyk A, Wojtkowski M. Fuchs' endothelial dystrophy in 830-nm spectral domain optical coherence tomography. *Ophthalmic Surg Lasers Imaging*. 2008;39:S83–S85.
12. Xia D, Zhang S, Nielsen E, et al. The ultrastructures and mechanical properties of the D descement's membrane in Fuchs endothelial corneal dystrophy. *Sci Rep*. 2016;6:4–10.
13. Briggs A, Kolosov O. Acoustic microscopy for imaging and characterization. *MRS Bull*. 1996;21:30–35.
14. Wickramasinghe HK. Contrast and imaging performance in the scanning acoustic microscope. *J Acoust Soc Am*. 1979;50:664–672.
15. Wickramasinghe HK. Scanning acoustic microscopy: a review. *J Mircosc*. 1983;129:63–73.
16. Yu Z, Boseck S. Scanning acoustic microscopy and its applications to material characterization. *Rev Mod Phys*. 1995;67:863–891.
17. Bereiter-Hahn J. Probing biological cells and tissues with acoustic microscopy. In: Briggs A, ed. *Advances in Acoustic Microscopy*. Boston: Springer; 1995:79–115.
18. Miura K, Yamamoto S. A scanning acoustic microscope discriminates cancer cells in fluid. *Sci Rep*. 2015;3:15243.
19. Hofmann M, Pflanzer R, Habib A, et al. Scanning acoustic microscopy—a novel noninvasive method to determine tumor interstitial fluid pressure in a xenograft tumor model. *Transl Oncol*. 2016;9:179–183.
20. Ahmed Mohamed ET, Kamanyi AE, Pluta M, Grill W. Age-dependent acoustic and microelastic properties of red blood

cells determined by vector contrast acoustic microscopy. *Microsc Microanal*. 2012;18:436–444.

21. Kolosov OV, Levin VM, Mayev RG, Senjushkina TA. The use of acoustic microscopy for biological tissue characterization. *Ultrasound Med Biol*. 1987;13:477–483.
22. Bereiter-Hahn J, Blase C, Kundu T, Wagner O. Cells as seen with the acoustic microscope. *Acoust Imaging*. 2002;26:83–90.
23. Brand S, Weiss EC, Lemor RM, Kolios MC. High frequency ultrasound tissue characterization and acoustic microscopy of intracellular changes. *Ultrasound Med Biol*. 2008;34:1396–1407.
24. Beshtawi MI, Akhtar R, Hillarby MC, et al. Scanning acoustic microscopy for mapping the microelastic properties of human corneal tissue. *Curr Eye Res*. 2013;38:437–444.
25. Gremaud G. Scanning acoustic microscopy: SAM. *Materials Science Forum*. 2001;366–368:676–683.
26. Briggs A. *Acoustic Microscopy*. 2nd ed. Oxford: Clarendon Press; 1992:104–125.
27. Weiglein RD, Wilson RG. Characteristic material signatures by acoustic microscopy. *Electron Lett*. 1978;14:352–354.
28. Atalar A. An angular-spectrum approach to contrast in reflection acoustic microscopy. *J Appl Phys*. 1978;49:5130–5139.
29. Briggs A. Acoustic microscopy - a summary. *Rep Prog Phys*. 1992;52:851–909.
30. Li M, Feng Z. Accurate Young's modulus measurement based on Rayleigh wave velocity and empirical Poisson's ratio. *Rev Sci Instrum*. 2016;87:075111.
31. Dapena I, Moutsouris K, Droutsas K, Ham L, van Dijk K, Melles GRJ. Standardized "no-touch" technique for Descemet membrane endothelial keratoplasty. *Arch Ophthalmol*. 2011;129:88–94.
32. Dapena I, Ham L, Droutsas K, Van Dijk K, Moutsouris K, Melles GRJ. Learning curve in Descemet's membrane endothelial keratoplasty: first series of 135 consecutive cases. *Ophthalmology*. 2011;118:2147–2154.
33. McCarey BE, Edelhauser HF, Lynn MJ. Review of corneal endothelial specular microscopy for FDA clinical trials of refractive procedures, surgical devices, and new intraocular drugs and solutions. *Cornea*. 2008;27:1–16.
34. Atalar A, Quate CF, Wickramasinghe HK. Phase imaging in reflection with the acoustic microscope. *Appl Phys Lett*. 1977;31:791–793.
35. Scruby CB, Jones KR, Antoniazzi L. Diffraction of elastic waves by defects in plates: Calculated arrival strengths for point force and thermoelastic sources of ultrasound. *J Nondestruct Eval*. 1986;5:145–156.
36. Malischewsky PG, Tuan TT. A special relation between Young's modulus, Rayleigh-wave velocity, and Poisson's ratio. *J Acoust Soc Am*. 2009;126:2851–2853.
37. Tittmann BR, Xi X. Imaging and quantitative data acquisition of biological cell walls with atomic force microscopy and scanning acoustic microscopy. In: Mèndez-Vilas A, ed. *Microscopy: Advances in Scientific Research and Education*. Badajoz: Formatex Research Center; 2014:161–172.
38. Hess P. Surface acoustic waves in material science. *Phys Today*. 2002;55:42–47.
39. Liang K, Bennett SD, Khuri-Yakub BT, Kino GS. Precision measurement of Rayleigh wave velocity perturbation. *Appl Phys Lett*. 1982;41:1124–1126.
40. Maebayashi M, Matsuoka T, Koda S, Hashitani R, Nishio T, Kimura SI. Evaluation of Young's modulus for polymer thin film on isotropic substrate by complex V(z) curve. *Jpn J Appl Phys*. 2004;43:2920–2923.
41. Gandhi S, Jain S. *The Anatomy and Physiology of Cornea. Keratoprostheses and Artificial Corneas: Fundamentals and Surgical Applications*. Berlin - Heidelberg: Springer; 2015:19–25.
42. Lewis PN, White TL, Young RD, Bell JS, Winlove CP, Meek KM. Three-dimensional arrangement of elastic fibers in the human corneal stroma. *Exp Eye Res*. 2016;146:43–53.
43. Kenney MC, Labermeier U, Hinds D, Waring GO. Characterization of the Descemet's membrane/posterior collagenous layer isolated from Fuchs' endothelial dystrophy corneas. *Exp Eye Res*. 1984;39:267–277.
44. Johnson H, Bourne WM, Jean R. The ultrastructure of Descemet's Membrane. *Arch Ophthalmol*. 1982;100:1942–1947.
45. del Buey MA, Cristóbal JA, Ascaso FJ, Lavilla L, Lanchares E. Biomechanical properties of the cornea in fuchs' corneal dystrophy. *Invest Ophthalmol Vis Sci*. 2009;50:3199–3202.
46. Wacker K, McLaren JW, Kane KM, Baratz KH, Patel SV. Corneal hydration control in fuchs' endothelial corneal dystrophy. *Invest Ophthalmol Vis Sci*. 2016;57:5060–5065.
47. Mandell RB, Polse KA, Brand RJ, Vastine D, Demartini D, Flom R. Corneal hydration control in fuchs' dystrophy. *Invest Ophthalmol Vis Sci*. 1989;30:845–852.
48. Xia D, Zhang S, Hjortdal JØ, Li Q, Thomsen K, Chevallier J. Hydrated human corneal stroma revealed by quantitative dynamic atomic force microscopy at nanoscale. *ACS Nano*. 2014;8:6873–6882.

Investigative Ophthalmology & Visual Science